芸術科学会論文誌 Vol. 13, No. 1, pp. 1 – 10

流体における剛体の実時間シミュレーション

謝 浩然 (非会員)　宮田 一乗 (正会員)

北陸先端科学技術大学院大学

Langevin Rigid: Animating Immersed Rigid Bodies in Real-time

Haoran Xie　Kazunori Miyata

Japan Advanced Institute of Science and Technology

{xiehr, miyata} @ jaist.ac.jp

概要

本論文では，非圧縮粘性流体における剛体運動の実時間シミュレーション手法である Langevin rigid 法を提案する．提案手法では，リアルな流体における剛体運動を再現するため，一般化されたキルヒホッフ方程式を用いて，剛体のまわりの流れからの剛体に対する力とトルクを考慮する．本提案法は，剛体と流体との境界面で生じた乱流の影響に対して一般化されたランジュバン方程式を利用するので，Langevin rigid 法と名付ける．Langevin rigid 法は流体の付加質量の影響と乱流モデルによる粘性負荷を事前処理にして，ランタイムではリジッドボディソルバのみを実行するため，提案手法が流体における複雑な剛体の挙動を実時間的にシミュレーションできる．さらに，高レイノルズ流体における葉っぱや紙切れなどの様々な形状の軽量剛体のリアルなシミュレーションが可能になる．

Abstract

We present the *Langevin rigid* approach, a technique for animating the dynamics of immersed rigid bodies in viscous incompressible fluid in real-time. We use generalized Kirchhoff equations to ensure forces and torques from the surrounding fluid that create realistic motion of immersed rigid bodies. We call our method the *Langevin rigid* approach because the generalized Langevin equations are applied to represent the effects of turbulent flow generated at the body surface. The Langevin rigid approach precomputes added-mass effects and the vortical loads from turbulent model, and executes the rigid body solver in runtime, so that this method is straightforward and efficient to the interactive simulations. Many types of rigid bodies with lightweight mass (e.g. leaf or paper) can be simulated realistically in high-Reynolds-number flows.

1 Introduction

Rigid body simulations are the fundamental techniques in computer animation, which are ubiquitously used in various applications. Although current rigid-body solvers can handle the body dynamics and collisions sophisticatedly, it remains a challenging work to simulate immersed rigid-body dynamics, which considers the motion of rigid bodies fully immersed in air or submerged underwater. In our daily-life, we notice that a paper moving through air follows a beautiful but chaotic-like trajectory rather than a straightforward vertical path.

The motion of immersed rigid body can be characterized by a Reynolds number Re and its mean falling velocity U_0.

$$Re = \frac{U_0 d}{\nu}; \qquad U_0 = \sqrt{(\frac{\rho_b}{\rho_s} - 1)gb} \tag{1}$$

where ν is the kinematic viscosity of the surrounding fluid; d and b are the characteristic length and thickness of the rigid body; ρ_b and ρ_f are the densities of rigid body and fluid separately. For a common leaf moving in air, Re is greatly high at a magnitude of 10^4. In the case of a high-Reynolds-number flow, the vortices born around the body and then detach from body surface as vortex shedding. The immersed rigid-body dynamics is so unsteady with path instabilities that the simulations of immersed rigid bodies become notoriously difficult in the field of both fluid mechanics and computer graphics.

In contrast to the conventional two-way coupling simulations, high-Re two-way coupling is far complicated where the strong-coupled motions between rigid bodies and flow cannot be understood without fine details of fluid motion, i.e. vortex-body interaction. To the best of authors' knowledge, the technique for simulating high-Re two-way coupling of immersed rigid bodies is absent in computer animation with the following reasons: 1) The computation of coupling motions with fluid in small grids is too heavy for graphical applications; 2) While simulating flow in high resolutions, the turbulent motions and numerical dissipation are hard to be analyzed; 3) In order to achieve stable simulation results, the implementation involving boundary conditions requires infinitesimal time steps. Therefore, it is impossible to simulate immersed rigid bodies by conventional coupling approaches. To resolve this issue, we utilize generalized Kirchhoff equations with detailed analysis of the flow effects from the surrounding flow.

The research motivation of this work is to supply a plausible simulation approach of immersed rigid-body dynamics in real-time on CPU. Because this is a great challenging problem to account for turbulent flow for real-time simulations, we assume that the body is thought as a passive particle in the fluid flow with the mean falling velocity of the body whereas the real situation is a body moving through the still flows, so that the implementation of turbulent energy need not handle body's boundary conditions and can be executed in pre-processes. Due to the absence of boundary conditions, the aerodynamic drag and lift forces are resolved implicitly in this work. In contrast to the empirical model of aerodynamic forces based on quasi-steady assumptions, this approach can achieve visually plausible simulation results accounting for the viscous effects of unsteady forces from generated turbulence but lose physical accuracy as trade-off with computation cost.

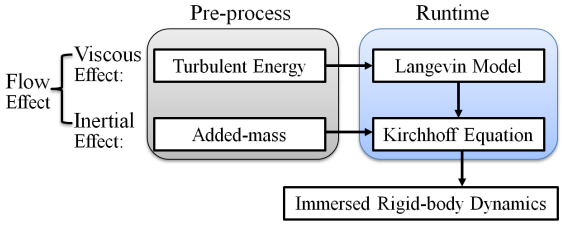

Figure 1: An illustration of our approach.

In term of our assumption, we propose a Langevin rigid approach as a tradeoff between the computation costs and simulation accuracy to resolve the dynamics of immersed rigid bodies [22]. As illustrated in Figure 1, our approach separates flow effect from the surrounding flow into 1) inertial effect from potential flow and 2) viscous effect from turbulent flow:

- For the inertial effect, we precompute the added-mass tensors due to both translational and rotational displacements of the surrounding flow.
- For the viscous effect, we calculate the turbulent energy and its dissipation rate for obtaining vortical loads on the body in a pre-process stage.

The vortical loads of viscous effect are represented in the Langevin model as a stochastic process of the object velocity, and then substituted into Kirchhoff equations with added-mass tensors. Our approach runs a rigid body solver to solve generalized Kirchhoff equations in runtime process. Overall, the proposed approach makes it feasible to efficiently simulate immersed rigid bodies with arbitrary shapes in low computation costs. The major contributions of this work are summarized as follows:

- A new method based on generalized Langevin equations of both translational and rotational velocities to represent the characteristics of the surrounding flow whereas previous work [5, 24] did not account for the dynamics of rigid bodies and the coupling between translational and rotational velocities.

- A new representation of rigid body dynamics as generalized Kirchhoff equation in body-fixed frame to account for both inertial and viscous effects, which is different from previous work [21] where only inertial effect was considered.
- A two-stage framework includes pre-processes stage of added-mass effects and the k-ε turbulent model, and runtime stage of rigid body solver, which is shown to be efficient to simulate immersed body dynamics in real-time.

The rest of this paper is organized as follows: Section 2 highlights some research topics related to immersed rigid-body dynamics. Section 3 details the equations of rigid body by generalized Kirchhoff equations. Section 4 explains the Langevin model to capture the motion in a stochastic process way, and Section 5 describes the approach on how to obtain turbulent parameters from the k-ε turbulent model. Section 6 specifies the algorithms used in the implementation of the proposed approach. Section 7 shows the simulation results of different objects by our Langevin rigid approach. Finally, we conclude this paper with a discussion of possible future work in Section 8.

2 Related Work

Two-way Coupling between rigid body and incompressible fluid has been studied extensively in computer graphics. Basically there are two types of schemes on this research. The first scheme handles fluid in Euler formulation and rigid bodies in Lagrangian formation [1, 4, 6, 9]. Guendelman et al. [9] proposed a robust ray casting algorithm for the coupling between fluid and cloths to avoid fluid leaking. Carlson et al. [4] treated the rigid body as fluid grid by using distributed Langrange multiplier. The second scheme is the fully Langrangian meshless method [2, 7, 18]. Becker et al. [2] proposed a direct forcing method in a predictor-corrector scheme with SPH particles. Solenthaler et al. [18] used a penalty method to analyze the forces on the immersed boundary. All these methods handle two-way coupling simulations in low-Re conditions. For our research purpose of immersed rigid-body dynamics, it is trivial and impossible to simulate high-Re two-way coupling with turbulent flow in computer graphics as explained in previous section.

Turbulent Flow The simulation of turbulent flows is different with direct numerical simulation of Navier-Stokes equations. First, from the view of fluid mechanics, there are some sophisticate approaches in this fields, including turbulent-viscosity models (k-ε equations), Reynolds-stress models, Probability Density Function methods (Langevin model) and large-eddy simulation. It is not apparent to adopt these approaches directly in computer animation, and there are some successful works [14, 15] in computer graphics community recently. Note that Langevin model is an empirical model based on k-ε equations [16, 17] but an effective Langragian-stochastic approach to represent the dynamics of passive particles in turbulent flow [13]. Recent work shows that non-spherical particles moving in turbulent flow [25] exhibit the similar dynamics of immersed rigid bodies which has been discussed in previous work [23]. Therefore, it is physically reasonable to adopt Langevin model for simulating immersed rigid bodies while following our assumption in this work.

Unsteady Dynamics A similar work [21] introduced a Kirchhoff tensor to represent inertial effects for underwater rigid body simulations. This approach is only suitable for the inviscid and irrotational flow with low-Re number. In this paper, we propose a Langevin model related to the turbulent flow for solving the vortical loads. Langevin model has been applied to enhance turbulent flow simulations [5] and simulations of floating lightweight rigid body [24] in previous work. In these work, the rotational velocity and the coupling between translational and rotational velocities are not concerned. We resolve these issues by combing generalized Kirchhoff equations with Langevin model in this paper.

3 Equations of Motion

Let us consider a rigid body of mass m, and center of mass O moving through a still fluid flow. The motion of the rigid body is described by $(R(t), \boldsymbol{x}(t))$. $R(t)$ represents the orientation of the body as a 3×3 orthogonal matrix rather than a quaternion form, and $\boldsymbol{x}(t)$ is the position of O at time step t in inertial reference frame. We represent the dynamic equations of motion in body-fixed frame. All symbols used throughout this paper can be found in Table 1.

3.1 Kinematic Equation

The translational and angular velocities of the object $(\boldsymbol{v}, \boldsymbol{\omega}) \in \mathbb{R}^6$ are given in body-fixed frame as follows:

$$\dot{R} = R\hat{\boldsymbol{\omega}}, \qquad \dot{\boldsymbol{x}} = R\boldsymbol{v} \tag{2}$$

where the operator $\hat{}: \mathbb{R}^3 \to so(3)$ is defined as $\boldsymbol{s}\hat{\boldsymbol{\omega}} = \boldsymbol{s} \times \boldsymbol{\omega}, \forall \boldsymbol{s} \in \mathbb{R}^3$, where the space $so(3)$ is the Lie algebra of the Lie group $SO(3)$. $\hat{\omega}$ is defined as

$$\begin{pmatrix} 0 & -\omega(3) & \omega(2) \\ \omega(3) & 0 & -\omega(1) \\ -\omega(2) & \omega(1) & 0 \end{pmatrix} \tag{3}$$

where $\omega(n)$ is the n-th element of angular velocity $\boldsymbol{\omega}$.

Table 1: Notation used through this paper(Bold letters denote vector variables.).

symbol	description
R	rotation matrix of body
$\boldsymbol{x}$	position of body
$\boldsymbol{\omega}$	angular velocity
$\boldsymbol{v}$	translational velocity
m	mass of body
$\boldsymbol{r}$	center of buoyancy
$\boldsymbol{g}$	gravitational acceleration
V	volume of body
ρ_b	body density
ρ_f	fluid density
ν	kinematic viscosity of fluid
Re	Reynolds number
$\boldsymbol{F}_t$	force due to turbulence
$\boldsymbol{F}_g$	force due to gravity
$\boldsymbol{\Gamma}_t$	torque due to turbulence
$\boldsymbol{\Gamma}_g$	torque due to gravity
M_f	added mass tensor
M	mass tensor
J_f	added inertia tensor
J	inertia tensor
J_0	moment of inertia
U_0	mean falling velocity of body
k	turbulent kinetic energy
ϵ	dissipation rate of turbulent energy
χ	turbulent frequency $\chi = \varepsilon/k$
$\boldsymbol{u}$	fluid velocity
$\langle \boldsymbol{u} \rangle$	mean flow velocity
α	relaxation rate coefficient
β	diffusion coefficient
$\boldsymbol{W}$	Wiener process in $\mathbb{R}^3$
$\boldsymbol{\xi}$	normal Gaussian distributed variable
Δt	time step of simulation

3.2 Dynamic Equation

The dynamics of a rigid body immersed in a viscous fluid results from the coupling between the body and the surrounding flow. The dynamical effects from the interaction of the fluid to a body displacement, including both translational and rotational transformations, are described as added-mass tensors M_f and J_f. M_f represents the force and torque due to the fluid coupling to a translational acceleration of the body and J_f is to a rotational acceleration. Therefore, the body dynamics is governed by the generalized Kirchhoff equations [8]. The dynamic equation has the following form in body-fixed frame.

$$\begin{aligned} M \cdot \dot{\boldsymbol{v}} + \boldsymbol{v} \times (M \cdot \boldsymbol{\omega}) &= \boldsymbol{F}_t + \boldsymbol{F}_g \\ J \cdot \dot{\boldsymbol{\omega}} + \boldsymbol{\omega} \times (J \cdot \boldsymbol{\omega}) + \boldsymbol{v} \times (M_f \cdot \boldsymbol{v}) &= \boldsymbol{\Gamma}_t + \boldsymbol{\Gamma}_g \end{aligned} \quad (4)$$

where $M = mI + M_f$, $J = J_0 + J_f$, J_0 is the moment of inertia of the body and I is the 3×3 identity matrix. $\boldsymbol{F}_t$ and $\boldsymbol{\Gamma}_t$ are the resulted force and torque due to the turbulence generated at the body surface while the body moves in a viscous flow; $\boldsymbol{F}_g$ and $\boldsymbol{\Gamma}_g$ result from the buoyancy-corrected gravity.

Because the added-mass tensors are only determined by the body's geometry and independent of the generated turbulence at body surface [10], M_f and J_f can be computed in a precomputation step similar to the implementations of the mass tensor and rotational inertia tensor in [21].

The gravity and buoyancy act on the immersed rigid body with inverse directions. We express them in body-fixed frame as follows:

$$\boldsymbol{F}_g = R^T(m - \rho_f V)\boldsymbol{g} \quad (5)$$

$$\boldsymbol{\Gamma}_g = \rho_f V \boldsymbol{r} \times R^T \boldsymbol{g} \quad (6)$$

where $V = m/\rho_b$ is the volume of the body and $\boldsymbol{r}$ is the vector from the center of mass to the center of buoyancy in body-fixed frame.

The difficulty of solving Eq.(4) is to how to determine the force $\boldsymbol{F_t}$ and torque $\boldsymbol{\Gamma_t}$ due to surrounding turbulent flow, which causes path instability of the body in a chaotic way. We will describe the approach to specify vortical loads (force and torque) in the next section.

4 Langevin Model

The stochastic model for the motion of suspended fluid particles is proposed by Langevin decades ago. The velocity increments of a particle in continuous time steps are in highly correlated process, which is called the Ornstein-Unlebeck process [19]. The model can be applied to describe the Brownian motion of lightweight objects undergoing the vortical loads from the surrounding turbulent flow [13, 24].

For a statistically isotopic turbulence, the Langevin equation can be defined as the following stochastic differential equation:

$$d\boldsymbol{u}(t) = -\alpha \boldsymbol{u}(t) dt + \beta d\boldsymbol{W} \quad (7)$$

where $\boldsymbol{u}(t)$ is the translational velocity of a fluid particle; α and β are the relaxation rate and the diffusion coefficient, which reveal the properties of the turbulent flow; and $\boldsymbol{W}$ is a Wiener process which represents a Brownian motion with a continuous-time stochastic process. In this implementation, the process is calculated by a normal distribution with mean of zero and variance of the time interval Δt.

For a fluid particle with arbitrary shape, the relaxation term in Eq.(7) has no effect to angular velocity increments of the body as a rotational Brownian motion [13]. The Langevin equation for angular velocity is given as:

$$d\boldsymbol{\omega}(t) = \beta d\boldsymbol{W} \quad (8)$$

4.1 Generalized Langevin Equation

Pope [16] described the generalized Langevin equation for the suspended particle in a turbulent flow. The equation gives the expressions of α and β having the following forms:

$$\alpha = (\frac{1}{2} + \frac{3}{4}C_0)\frac{\varepsilon}{k}, \qquad \beta = (C_0\varepsilon)^{\frac{1}{2}} \tag{9}$$

where k and ε are kinetic energy and its dissipation rate of the surrounding turbulent flow; C_0 is a Kolmogorov coefficient. According to the Kolmogorov hypothesis, C_0 is related to the Reynolds number Re of the flow [17].

$$C_0(Re) = 6.5(1 + 140Re^{-\frac{4}{3}})^{-\frac{3}{4}} \tag{10}$$

For high-Reynolds-number flow ($Re > 10^3$), this relation is empirically fitted.

Finally, the dynamic equations of immersed body are discretized through finite-difference scheme by substituting Eqs.(7)(8)(9) into Eq.(4).

$$\begin{aligned}\boldsymbol{v}(t+\Delta t) - \boldsymbol{v}(t) = M^{-1}(&-\boldsymbol{v}(t) \times (M\boldsymbol{\omega}(t))\Delta t \\ &-\chi(\tfrac{1}{2} + \tfrac{3}{4}C_0)\boldsymbol{v}(t)\Delta t \\ &+(C_0\varepsilon\Delta t)^{\frac{1}{2}}\boldsymbol{\xi}_1 + \boldsymbol{F}_g(t)\Delta t)\end{aligned} \tag{11}$$

$$\begin{aligned}\boldsymbol{\omega}(t+\Delta t) - \boldsymbol{\omega}(t) = J^{-1}(&-\boldsymbol{\omega}(t) \times (J\boldsymbol{\omega}(t))\Delta t \\ &-v(t) \times (M_f\boldsymbol{v}(t))\Delta t \\ &+(C_0\varepsilon\Delta t)^{\frac{1}{2}}\boldsymbol{\xi}_2 + \boldsymbol{\Gamma}_g(t)\Delta t)\end{aligned} \tag{12}$$

where $\chi = \varepsilon/k$ is the turbulent frequency; $\boldsymbol{\xi}_1$ and $\boldsymbol{\xi}_2$ are the vectors of normal Gaussian distributed variables with mean zero and unit deviation as $Norm(0, 1)$. These two vectors are generated using the Box-Muller algorithm in our work.

The parameters (χ, ε) measure the characteristics of the surrounding turbulent flow. We pre-generate these parameters $(\chi(t), \varepsilon(t))$ by two-equation k-ε turbulent model in the next section.

5 Turbulence Model

In a turbulent flow, the fluid velocity $\boldsymbol{u}$ can be represented by Reynolds decomposition with the mean flow $\langle\boldsymbol{u}\rangle$ and fluctuating velocity $\boldsymbol{u}'$ ($\boldsymbol{u} = \langle\boldsymbol{u}\rangle + \boldsymbol{u}'$). The common approach for solving the fluid-rigid coupling problem based on the three dimensional Navier-Stokes equations are extremely computationally expensive, because the fluctuations of turbulence would be of small scale and high frequency. It is obvious not suitable for an interactive application. The most widely used turbulence model is the k-ε turbulent model proposed in [12], which requires low computational cost. The k-ε model is a semi-empirical model based on the transport equations, which consist of two coupled equations of the turbulent kinetic energy k and its dissipation rate ε. This energy transport equations are defined as follows:

$$\begin{aligned}D_t k &= \nabla \cdot ((\nu + \tfrac{v_T}{\sigma_k})\nabla k) + G - \varepsilon \\ D_t\varepsilon &= \nabla \cdot ((\nu + \tfrac{v_T}{\sigma_\varepsilon})\nabla\varepsilon) + \chi(C_1 G - C_2\varepsilon)\end{aligned} \tag{13}$$

where D_t denotes a Lagrangian derivative; σ_k and σ_ε are the turbulent Prandtl numbers for k and ε; C_1 and C_2 are empirical constants. The values of these parameters are given empirically as: $\sigma_k = 1.0$, $\sigma_\varepsilon = 1.3$, $C_1 = 1.44$ and $C_2 = 1.92$ [12].

The turbulent viscosity v_T in Eq.(13) describes the small scale turbulent motion as a viscous diffusion scale in the turbulent model. Turbulent viscosity v_T is defined as:

$$v_T = C_\mu\frac{k^2}{\varepsilon} \tag{14}$$

where $C_\mu = 0.09$ is an empirical constant.

The term G in Eq.(13) represents the generation of turbulent kinetic energy due to the mean velocity gradients and can be defined in terms of the strain tensor of the flow:

$$G = 2v_T\sum_{ij} S_{ij}^2 \tag{15}$$

where $S_{ij} = \frac{1}{2}(\frac{\partial\langle u\rangle_i}{\partial x_j} + \frac{\partial\langle u\rangle_j}{\partial x_i})$.

In our implementation, we simplify Eq.(13) by avoiding the calculations of the incorporated diffusion terms, which are proven to be visually unnecessary in previous work [14]. The transport equations have the following simplified formulations:

$$D_t k = G - \varepsilon \tag{16}$$

$$D_t\varepsilon = \chi(C_1 G - C_2\varepsilon) \tag{17}$$

In cases of high turbulent flows with high Reynolds numbers, the initial state (k_0, ε_0) is defined in terms of the mean falling velocity U_0 as described in Eq.(1) to estimate the information about the history of the moving body. The initial conditions for energy transport equations are given as follows:

$$k_0 = \frac{3}{2}U_0^2; \qquad \varepsilon_0 = C_\mu^{\frac{3}{4}}k_0^{\frac{3}{2}}l^{-1} \tag{18}$$

where l is the length scale of the MAC grid cell in the mean flow simulation.

The turbulent parameters (χ, ε) are explicitly solved with finite difference scheme from Eqs.(15)(16)(17) as shown in Figure 2, where a standard fluid solver is applied to obtain the mean velocities $\langle\boldsymbol{u}\rangle$ of the base flow. According to the Kolmogorov theory, for high Reynolds number, the initial turbulence is unstable and the kinetic energy is divided into smaller scales. After reaching a critical scale value, turbulent energy dissipates due to viscosity, creating an energy cascade [15]. Figure 2 shows the varying dissipate rate accompanying the kinetic energy in the calculated result.

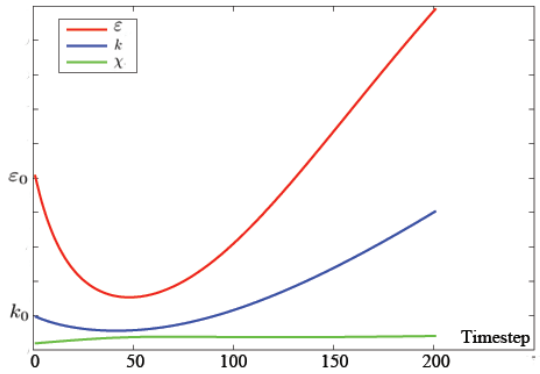

Figure 2: Turbulent parameters (χ, ε) in time steps with $Re = 3.8 \times 10^3$ and $32 \times 32 \times 16$ MAC grids.

6 Implementation

The implementation of our approach consists of two computation stages: pre-computations of added-mass tensors and turbulent flow; and runtime simulation of a rigid body solver as shown in Figure 1.

Turbulent flow The turbulent model is based on a standard fluid solver to resolve the mean flow around the body. However, the complicated solver of Reynolds-averaged Navier-Stokes equations is usually applied to the k-ε model for accurate solutions, the standard solver can be more visually plausible and efficient in computer graphics [15].

We utilize a typical MAC staggered grid with semi-Langragian advection to obtain the base mean flow as described in Algorithm 1, which is similar to previous work [5, 15]. The turbulent energy k and its dissipation rate ε are computed at each grid node. In this work, we consider the viscous effect from the surrounding flow by Lagrangian tracking a passive particle with the same position of rigid body in the fluid field, i.e. the implementation of boundary conditions of rigid body is not necessary, and the inflow velocity is chosen as the mean falling velocity of Eq.(1) and defined as:

$$U_{in} = U_0 \tag{19}$$

Although the implementation of the mean flow and turbulent energy could be in real-time by GPU for low-resolution, this computation should be executed offline because: 1) We only compute it once; 2) We need to guarantee the runtime computation of rigid body solver in real-time; 3) Other turbulent solver or high-resolution simulations are also acceptable in our framework.

Rigid body solver Our Langevin rigid approach is relatively efficient for real-time simulations, because the computation burdens involving turbulent flow effects are executed in pre-computation steps. The most runtime computation is for the rigid body solver, which is described in Algorithm 2. We apply a standard Runge-Kutta scheme for resolving the coupling dynamic equations, Eq.(11) and Eq.(12). In the work of [11], a lie group integrator of Euclidean motions is shown to be more robust than the Runge-Kutta scheme for large timesteps. Because our work focuses on the falling motion of immersed rigid bodies, we utilize a quite small scale of timestep for the rigid body solver. The Runge-Kutta scheme is efficient enough for our simulation.

Algorithm 1 Pseudo-code for pre-generated turbulent model.

```
Boundary conditions ←Eqs.(18)(19)
Timestep t = 0
while not stopped do
    // Mean flow ⟨u⟩
    Convection by semi-Lagrangian
    Pressure projection by Poisson solver

    // Energy transport
    Get turbulent viscosity v_T ←Eq.(14)
    Get strain tensor term G ←Eq.(15)
    Integrate turbulent energy k ←Eq.(16)
    Integrate dissipation rate ε ←Eq.(17)

    t = t + Δt
end while
Output: (χ, ε)
```

Algorithm 2 Pseudo-code for the runtime computation.

```
Precomputation of added-mass tensors
Initialization of rigid body
Timestep t = 0
while not arrive ground do
    Calculate gravity force←Eq.(5)
    Query χ_t and ε_t (Algorithm 1)
    Update translational velocity v ←Eq.(11)
    Update angular velocity ω ←Eq.(12)
    Integrate (R, x) ←Eq.(2)
    Render data
    t = t + Δt
end while
```

7 Results

In this section, we describe the simulation results using the proposed Langevin rigid approach.

A piece of paper released in air with different release angles is simulated by our approach as shown

in Figure 3. The cross section of the leaf model used in our simulation is elliptical (semi-major axis and minor axis are 4.0 and 1.0 cm respectively). The thickness is set to be 0.01 cm and the density number is 0.8. The Reynolds number (4.3×10^4) is so large that the turbulence can be generated at the paper surface. The paper falls down following a helical trajectory in Figure 3(a) and a side-to-side tumbling motion in Figure 3(b) which are in compliance with the analysis result in [23]. The trajectories have the secondary motions that the paper rotates around the major-axis while falling, which usually happens in reality. Note that we can not understand the simulation results in prior by our approach while the initial conditions are modified, e.g. release angle.

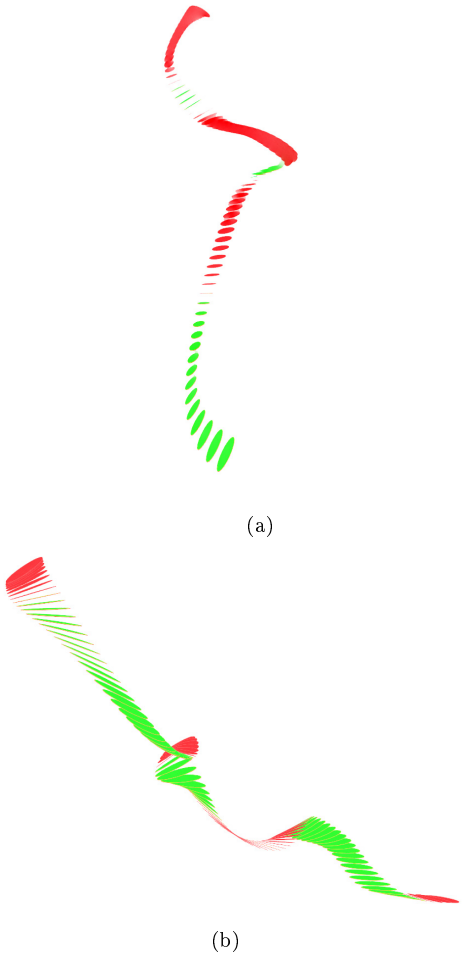

(a)

(b)

Figure 3: Simulation results of a piece of paper falling in air. (a) initial release angle = 75°; (b) initial release angle = 30°.

Figure 4 shows a comparison between our simulation and a video of a flying paper airplane.

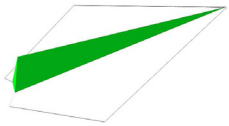

The paper airplane is made by a 8.3 × 8.3 × 0.01 (cm) print paper. The added-mass tensors and moment of inertia of the body depend on the geometries with closed shape, where the fold part of the paper airplane is constructed as volume as shown in the right figure. The simulation begins with an initial velocity of 20 cm/s in the horizontal direction, and the simulated result shows two turning motions (turning front and turning sideways) which are caused by the surrounding airflow. The turning motions are similar to the observation from ground truth in Figure 4.

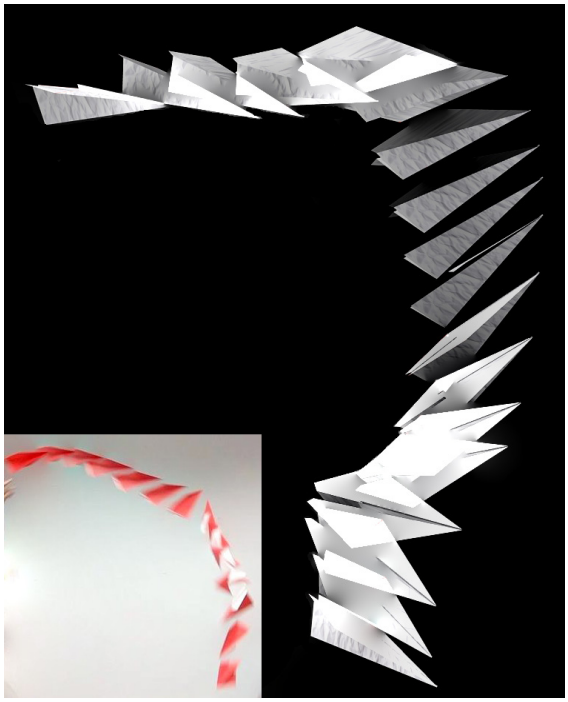

Figure 4: Comparison between the simulation and the ground truth of a flying paper airplane.

Figure 5 shows the discrete frames from the animation of a rubber ellipsoid falling in water, and the time interval is 50 ms. The rubber ellipsoid with semi-principal axes of length 1 cm, 2 cm and 4 cm falls down in a quiescent water flow. A small scale of fluttering motion can be found in Figure 5(a) using the simulation method of the previous work [21]. In contrast to this previous work, the coupling between forces and torques due to the surrounding turbulent flow can be indicated properly using our Langevin rigid approach. The oscillations of rigid body in differential directions from falling experiments (Figure 5(c)) are captured in our simulation, so that our

simulation result is more realistic than the previous work.

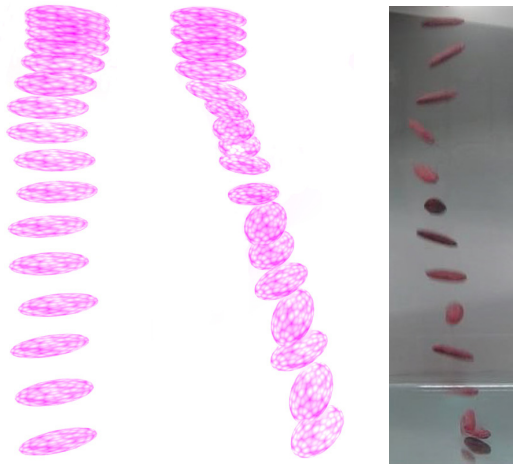

(a) (b) (c)

Figure 5: Comparison between (b) our simulation and (a) the previous work. In (a) only the added-mass tensors are embedded into the Kirchhoff equations, whereas our approach has concerned the force and torque from the surrounding turbulence (b). (c) Ground truth shows oscillations generated in different directions.

The precomputation time of added-mass tensors depends on the amount of the body meshes; and the precomputation time of turbulent model depends on the grid solutions of the base flow. In the case of 1280 meshes and $32 \times 32 \times 8$ MAC grid, the precomputation times are 53 ms and 182 ms, respectively. All simulations were implemented on an Intel Core i7 CPU with 3.20 GHz and 12.0 GB RAM. The simulation time for a single loop of runtime computation is not more than 2.0 ms. As shown in Table 2, the runtime computation time is independent of the body triangular meshes and time step, and it is suitable for real-time simulations.

Table 2: Computation cost of our simulation results on runtime.

bodies	meshes	timestep	avg cost
ellipsoid 1	320	1 ms	1.59 ms
ellipsoid 1	320	5 ms	1.63 ms
ellipsoid 1	320	10 ms	1.65 ms
ellipsoid 2	1280	5 ms	1.71 ms
piece of paper	1024	5 ms	1.73 ms
paper airplane	288	5 ms	1.86 ms

8 Conclusion

We presented the Langevin rigid approach for realistic simulations of rigid bodies in viscous, high-Reynolds-number flows. The main strength of the Langevin rigid method lies in combining Kirchhoff equations and Langevin model to represent the chaotic motions of immersed rigid bodies. The method allows a real-time simulation for interactive applications like game. Note that the method described in this paper is physics-based one, a cartoon-style animation is not considered here.

Limitations exist in the Langevin rigid approach. Because the simulation results are sensitive to the initial conditions as discussed in Section t, including release angle, velocities etc., the appropriate variables should be chosen to meet the ground truth in our simulation results. Some characteristic motions like fluttering and tumbling motions, are not apparently captured by the approximated turbulent model. These limitations can be improved by animation control strategies in future work.

Some fruitful avenues for future work remain. It is possible to extend this Langevin rigid approach to deformable rigid bodies and bubble dynamics. In this paper, the collisions among rigid bodies are not considered, which can be treated as external force and torque in this approach. In addition, the experimental results of falling rigid bodies indicate that six primitive trajectories exist, which can be applied to a motion synthesis approach for simulating the dynamics of immersed bodies [23]. It is promising to combine the Langevin rigid approach with motion synthesis method to achieve realistic and controllable simulations.

References

[1] C. Batty, F. Bertails, and R. Bridson. A fast variational framework for accurate solid fluid coupling. *ACM Trans. Graph.*, 26(3), July 2007.

[2] M. Becker, H. Tessendorf, and M. Teschner. Direct forcing for lagrangian rigid-fluid coupling. *IEEE Transactions on Visualization and Computer Graphics*, 15(3):493–503, May 2009.

[3] C. E. Brennen. A review of added mass and fluid inertial forces. *NASA STI/Recon Technical Report N*, 82:21535, Jan. 1982.

[4] M. Carlson, P. J. Mucha, and G. Turk. Rigid fluid: animating the interplay between rigid bodies and fluid. *ACM Trans. Graph.*, 23(3):377–384, Aug. 2004.

[5] F. Chen, Y. Zhao, and Z. Yuan. Langevin particle: A self-adaptive lagrangian primitive for flow simulation enhancement. *Computer Graphics Forum*, 30(2):435–444, 2011.

[6] N. Chentanez and M. Müller. Real-time simulation of large bodies of water with small scale details. In *Proceedings of the 2010 ACM SIGGRAPH/Eurographics Symposium on Computer Animation*, SCA '10, pages 197–206, Aire-la-Ville, Switzerland, Switzerland, 2010. Eurographics Association.

[7] S. Clavet, P. Beaudoin, and P. Poulin. Particle-based viscoelastic fluid simulation. In *Proceedings of the 2005 ACM SIGGRAPH/Eurographics symposium on Computer animation*, SCA '05, pages 219–228, New York, NY, USA, 2005. ACM.

[8] P. Fernandes, P. Ern, F. Risso, and J. Magnaudet. Dynamics of axisymmetric bodies rising along a zigzag path. *Journal of Fluid Mechanics*, 606:209–223, 6 2008.

[9] E. Guendelman, A. Selle, F. Losasso, and R. Fedkiw. Coupling water and smoke to thin deformable and rigid shells. *ACM Trans. Graph.*, 24(3):973–981, July 2005.

[10] M. S. Howe. On the force and moment on a body in an incompressible fluid, with application to rigid bodies and bubbles at high and low reynolds numbers. *The Quarterly Journal of Mechanics and Applied Mathematics*, 48(3):401–426, 1995.

[11] M. Kobilarov, K. Crane, and M. Desbrun. Lie group integrators for animation and control of vehicles. *ACM Trans. Graph.*, 28(2):16:1–16:14, May 2009.

[12] B. E. Launder and B. I. Sharma. Application of the energy-dissipation model of turbulence to the calculation of flow near a spinning disc. *Letters Heat Mass Transfer*, 1:131–137, Dec. 1974.

[13] M. Makino and M. Doi. Brownian Motion of a Particle of General Shape in Newtonian Fluid. *Journal of the Physical Society of Japan*, 73:2739, Oct. 2004.

[14] T. Pfaff, N. Thuerey, J. Cohen, S. Tariq, and M. Gross. Scalable fluid simulation using anisotropic turbulence particles. *ACM Trans. Graph.*, 29(6):174:1–174:8, Dec. 2010.

[15] T. Pfaff, N. Thuerey, A. Selle, and M. Gross. Synthetic turbulence using artificial boundary layers. *ACM Trans. Graph.*, 28(5):121:1–121:10, Dec. 2009.

[16] S. B. Pope. A lagrangian two-time probability density function equation for inhomogeneous turbulent flows. *Physics of Fluids*, 26(12):3448–3450, 1983.

[17] S. B. Pope. Simple models of turbulent flows. *Physics of Fluids*, 23(1):011301, 2011.

[18] B. Solenthaler, J. Schlafli, and R. Pajarola. A unified particle model for fluid solid interactions. *Comput. Animat. Virtual Worlds*, 18(1):69–82, Feb. 2007.

[19] G. E. Uhlenbeck and L. S. Ornstein. On the theory of the brownian motion. *Phys. Rev.*, 36:823–841, Sep 1930.

[20] S. Weissmann and U. Pinkall. Filament-based smoke with vortex shedding and variational reconnection. In *ACM SIGGRAPH 2010 papers*, SIGGRAPH '10, pages 115:1–115:12, New York, NY, USA, 2010. ACM.

[21] S. Weissmann and U. Pinkall. Underwater rigid body dynamics. *ACM Trans. Graph.*, 31(4):104:1–104:7, July 2012.

[22] H. Xie and K. Miyata. Langevin Rigid: Animating Immersed Rigid Bodies in Real-time. *Proc. of NICOGRAPH International 2013*, pages 89–96, 2013.

[23] H. Xie and K. Miyata. Real-time simulation of lightweight rigid bodies. *The Visual Computer 30*, 1, pages 81–92, 2014.

[24] Z. Yuan, F. Chen, and Y. Zhao. Stochastic modeling of light-weight floating objects. In *Symposium on Interactive 3D Graphics and Games*, I3D '11, pages 213–213, New York, NY, USA, 2011. ACM.

[25] M. Mando and L. Rosendahl. On the motion of non-spherical particles at high Reynolds number. *Powder Technology*, 202(1-3), Pages 1-13, 2010.

Haoran Xie

Haoran Xie is a Ph.D. candidate in the School of Knowledge Science, Japan Advanced Institute of Science and Technology (JAIST), Japan. He received his B.S. degree in the Department of Applied Mathematics, Anhui University, China in 2006. His current research interests include physics-based simulation and turbulence modeling in computer animation. He is a student member of IEEE and ACM SIGGRAPH.

Kazunori Miyata

Kazunori Miyata has been a Professor in the School of Knowledge Science at the Japan Advanced Institute of Science and Technology (JAIST) since 2002. Prior to joining JAIST, he was an Associate Professor in the Department of Imaging Art at the Tokyo Institute of Polytechnics. He received a B.S. degree from Tohoku University in 1984, and a M.S. and Ph.D. from the Tokyo Institute of Technology in 1986 and 1997. His research mainly focuses on rendering & modeling natural objects, texture generation, and multimedia applications. He is a member of ACM and IEEE.